

A Straightforward Frequency-Estimation Technique for GPS Carrier-Phase Time Transfer

Christine Hackman, Judah Levine, Thomas E. Parker, , , Dirk Piester, and Jürgen Becker

Abstract—Although Global Positioning System (GPS) carrier-phase time transfer (GPSCPTT) offers frequency stability approaching 10^{-15} at averaging times of 1 d, a discontinuity occurs in the time-transfer estimates between the end of one processing batch (1–3 d in length) and the beginning of the next. The average frequency over a multiday analysis period often has been computed by first estimating and removing these discontinuities, i.e., through concatenation. We present a new frequency-estimation technique in which frequencies are computed from the individual batches then averaged to obtain the mean frequency for a multiday period. This allows the frequency to be computed without the uncertainty associated with the removal of the discontinuities and requires fewer computational resources.

The new technique was tested by comparing the fractional frequency-difference values it yields to those obtained using a GPSCPTT concatenation method and those obtained using two-way satellite time-and-frequency transfer (TWSTFT). The clocks studied were located in Braunschweig, Germany, and in Boulder, CO. The frequencies obtained from the GPSCPTT measurements using either method agreed with those obtained from TWSTFT at several parts in 10^{16} . The frequency values obtained from the GPSCPTT data by use of the new method agreed with those obtained using the concatenation technique at $1 - 4 \cdot 10^{-16}$.

I. INTRODUCTION

GLOBAL POSITIONING SYSTEM (GPS) carrier-phase time transfer (GPSCPTT) has shown great promise over the past several years. In an experiment conducted between receivers located at the United States Naval Observatory (USNO, Washington, DC) and at Schriever Air Force Base (Colorado Springs, CO), Larson et al. [1] showed agreement between GPSCPTT and two-way satellite time-and-frequency transfer (TWSTFT) at a level of ± 1 ns over 96 d. Similarly, over the 6274 km baseline between USNO and the Physikalisch-Technische Bundesanstalt (PTB) in Braunschweig, Germany, Dach et al. [2] showed several-nanosecond-level agreement between GPSCPTT and TWSTFT over a period of about 180 d.

Manuscript received September 15, 2005; accepted March 17, 2006.

C. Hackman is with JILA, University of Colorado, Boulder, CO (e-mail: chackman@jila.colorado.edu).

J. Levine is with the Time and Frequency Division and JILA, National Institute of Standards and Technology and University of Colorado, Boulder, CO.

T. E. Parker is with the Time and Frequency Division, National Institute of Standards and Technology, Boulder, CO.

D. Piester and J. Becker are with Physikalisch-Technische Bundesanstalt, Braunschweig, Germany.

Bauch et al. [3] showed a frequency stability of $\sim 1 \cdot 10^{-15}$ at an averaging time of 1 d for the difference between GPSCPTT and TWSTFT measurements obtained using receivers located at the National Physical Laboratory (Teddington, UK), Observatoire de Paris (Paris, France), and Istituto Elettrotecnico Nazionale Galileo Ferraris (Torino, Italy), a network several hundred kilometers in span.

Despite this, a problem still exists when computing the fractional frequency difference between two clocks by means of GPSCPTT estimates, which is, a discontinuity occurs in the time-transfer estimates between the end of one GPSCPTT processing batch and the beginning of the next. Batches are typically 1–3 d in length; these steps generally range in size from 100 ps to 1 ns. The steps are thought to be caused by pseudorange noise [2]. The fact that one can observe a discontinuity between two sets of time-transfer estimates indicates that the pseudorange noise in either batch has not been averaged down enough to become smaller than the other sources of noise within each batch. In other words, all of the time-transfer estimates within one batch are subject to the same bias due to the remaining pseudorange noise, and the scatter between the individual points within a batch does not reflect this. The size of the steps between batches depends on the level of pseudorange noise at the sites [4] and on how well the pseudorange noise was averaged down in the GPSCPTT data analysis.

If the goal of a GPSCPTT experiment is to create a continuous set of time-transfer estimates representing the time difference between two clocks, then it is necessary either to align the discontinuous results by estimating and removing the discontinuities (the concatenation technique) or to avoid the creation of the discontinuities altogether by using a continuous processing method such as [5], [6]. However, if the goal is to estimate the fractional frequency difference between the clocks, then it should be possible to take a simpler approach: to estimate this frequency¹ directly from each batch of independently processed time-transfer estimates, then to combine these frequency estimates in order to obtain a mean frequency value for the period of interest. We test that idea in this paper and compare the frequency values obtained to those obtained using a concatenation technique. Of particular interest is

¹Henceforth, we shall refer to the fractional frequency difference between two clocks as simply the frequency or frequency difference.

the comparison of the frequencies of cesium fountain frequency standards. A cesium fountain realizes the SI second with a fractional frequency uncertainty of approximately $1 \cdot 10^{-15}$. The noise of a frequency comparison, therefore, must be smaller than this.

There are three advantages to the new technique. The first is that the frequency can be estimated for multiday periods without introducing the uncertainty associated with the concatenation process, which is discussed further in Sections II and V. The second is ease of computation. Although most concatenation techniques require that portions of the GPSCPTT measurements be processed twice, the new technique does not require this. Third, the new technique can be applied to time-transfer estimates produced by virtually any software package.

To test the proposed frequency-estimation technique, a GPSCPTT experiment was conducted between frequency standards located at the National Institute of Standards and Technology (NIST) in Boulder, CO and at PTB in Braunschweig, Germany. TWSTFT also was performed between these standards. The frequency difference between the clocks was computed from the GPSCPTT time-transfer estimates by use of both a concatenation method and the new technique. The frequency values obtained from these two methods were compared to each other and to the values obtained from TWSTFT.

II. THEORY

The method by which one computes a frequency from a single batch of time-transfer estimates will depend on the noise spectrum exhibited by those time-transfer estimates. For example, if the noise type is white frequency modulation (WHFM), the optimal frequency estimate will be obtained by computing a frequency from each of the adjacent time-transfer estimates and computing the simple mean of all of the frequency values. In practice, this can be accomplished by the mathematically equivalent technique of subtracting the first time-transfer estimate of the series from the last estimate and dividing by the time elapsed between them [7]. For batch j consisting of N_{es} time-transfer estimates $x_{j,1}, x_{j,2}, \dots, x_{j,i} \dots, x_{j,N_{es}}$ separated by time intervals Δt , the optimal mean frequency estimate y_j can be computed using:

$$y_j = \frac{1}{N_{es} - 1} \sum_{i=1}^{N_{es}-1} y_{j,i} \quad (1a)$$

$$= \frac{1}{N_{es} - 1} \sum_{i=1}^{N_{es}-1} \frac{x_{j,i+1} - x_{j,i}}{\Delta t} \quad (1b)$$

$$= \frac{x_{j,N_{es}} - x_{j,1}}{\Delta t [N_{es} - 1]}. \quad (1c)$$

The method by which one optimally combines the frequencies computed from the batches in order to obtain a mean frequency over a multiday period will again depend on the component of the noise spectrum that dominates at that period. Some clocks (e.g., hydrogen masers) to be

studied with GPSCPTT exhibit a WHFM spectrum at averaging times of 1–5 d [8]. High-quality commercial cesium standards exhibit WHFM at averaging times as long as tens of days [8], [9]. Therefore, in this paper, the mean frequency for a multiday period will be computed using techniques optimal for WHFM. In fact, we will take equations (1a)–(1c), which we have just used to compute the frequency from a single batch of GPSCPTT estimates, and generalize them in order to compute the mean frequency for multiday periods. When testing the new method, the mean frequency for a multiday period will be computed by calculating a frequency from each of the daily GPSCPTT batches, then computing the mean of the daily frequency values that lie within the period of interest. This is analogous to (1a). In contrast, when estimating frequency for a multiday period from a set of concatenated time-transfer estimates, the frequency will be computed by subtracting the first and last of the concatenated time-transfer estimates for that period and dividing by the time interval between them. This is analogous to (1c).

Let y_{mer} represent a frequency computed by use of a concatenation (merge) technique. The uncertainty of y_{mer} , represented by the statistical distribution $u_{y_{mer}}$, can be modeled as follows. Let:

$$y_{mer} = \frac{x'_{N,N_{es}} - x'_{1,1}}{N\tau_0}, \quad (2)$$

where $x'_{N,N_{es}}$ and $x'_{1,1}$ represent the last and first time-transfer estimates of the concatenated series (the prime mark is used to distinguish the concatenated time-transfer estimates from the unconcatenated ones), $\tau_0 (\equiv (N_{es} - 1) \cdot \Delta t)$ represents the length of each batch (typically 24 h) and N represents the number of batches that have been concatenated in order to form the time series.

Define our concatenation process as:

$$x'_{r+n,k} - x'_{r,l} = x_{r+n,k} - x_{r,l} - \sum_{j=r}^{r+n-1} m_j, \quad (3)$$

where m_j represents the discontinuity that is estimated and removed from between the j^{th} and $(j+1)^{th}$ batches. Note that, if $n = 0$, $x_{r+n,k}$ and $x_{r,l}$ are in the same batch, no discontinuity occurs between them, the summation is not invoked, and $x'_{r+n,k} - x'_{r,l} = x_{r+n,k} - x_{r,l}$. In other words, (3) defines a concatenation process that does not alter the relative position of time-transfer estimates within a batch. Rather, it moves all of the time-transfer estimates in a given batch “up” or “down” by the same amount.

Using (3), we see that:

$$x'_{N,N_{es}} - x'_{1,1} = x_{N,N_{es}} - x_{1,1} - \sum_{j=1}^{N-1} m_j, \quad (4)$$

and hence (2) becomes:

$$y_{mer} = \frac{x_{N,N_{es}} - x_{1,1} - \sum_{j=1}^{N-1} m_j}{N\tau_0}. \quad (5)$$

Let u_m represent the uncertainty in the estimate of each day-boundary discontinuity. Let u_x represent the noisiness of the time-transfer estimates within a single batch relative only to each other. In other words, u_x does not account for the time bias that is common to all time-transfer estimates in a batch. Using (5), we write:

$$\begin{aligned} u_{y_{\text{mer}}}^2 &= \frac{u_{x_{N,N_{\text{es}}}}^2 + u_{x_{1,1}}^2 + [N-1]u_m^2}{[N\tau_0]^2} \\ &= \frac{2u_x^2 + [N-1]u_m^2}{[N\tau_0]^2}. \end{aligned} \quad (6)$$

We have made two assumptions in (6). First, we have set the cross-correlation term $u_{x_{N,N_{\text{es}}}x_{1,1}}$ equal to zero. This seems reasonable if $N \neq 1$, because then the two estimates are from different, independently processed batches. Second, we have assumed that discontinuity estimates m_j and m_k share no correlated errors (i.e., $u_{m_j,m_k} = 0$). Discontinuities often are computed by producing overlapped sets of time-transfer estimates (e.g., batch 1 includes [21:00, day 1 – 2:55, day 3], batch 2 includes [21:00, day 2 – 2:55, day 4]) and computing the differences between the time-transfer estimates in the overlapped portion. If portions of a single batch are used to compute two discontinuity values (e.g., the discontinuities that precede and follow that batch), and if the estimates within that single batch have correlated errors ($u_{x_j,sx_{j,t}} \neq 0$), then it is possible that the two discontinuities estimated using this single batch will have correlated errors as well, i.e., that $u_{m_j,m_k} \neq 0$.

The uncertainty of a frequency estimated using the new “average” technique, y_{ave} , can be modeled as follows. Let:

$$y_{\text{ave}} = \frac{\sum_{j=1}^N y_j}{N}, \quad (7)$$

where y_j is the frequency computed from the j^{th} batch and N is the number of batches averaged. Again, this is analogous to (1a). If we assume that the errors in computing a frequency from batch j are uncorrelated to the errors in computing a frequency from batch k , we can write:

$$u_{y_{\text{ave}}}^2 \approx \frac{\sum_{j=1}^N u_{y_j}^2}{N^2}. \quad (8)$$

If, using (1c), we write:

$$y_j = \frac{x_{j,N_{\text{es}}} - x_{j,1}}{[N_{\text{es}} - 1] \Delta t} = \frac{x_{j,N_{\text{es}}} - x_{j,1}}{\tau_0}, \quad (9)$$

then:

$$u_{y_j}^2 = \frac{u_{x_{j,N_{\text{es}}}}^2 + u_{x_{j,1}}^2 - 2u_{x_{j,N_{\text{es}}}x_{j,1}}}{\tau_0^2} = \frac{2u_x^2}{\tau_0^2}, \quad (10)$$

where we have assumed that $u_{x_{j,N_{\text{es}}}x_{j,1}} = 0$. Substituting (10) into (8) yields:

$$u_{y_{\text{ave}}}^2 = \frac{2u_x^2}{N\tau_0^2}. \quad (11)$$

Eq. (6) and (11) imply that if $u_m < \sqrt{2} \cdot u_x$, y_{mer} will have a smaller uncertainty than y_{ave} .

There are different techniques for concatenating sets of time-transfer estimates. The simplest is to connect the last estimate of one set to the first estimate of the next set. In this case, $u_m = \sqrt{2} \cdot u_x$. The purpose in using a more sophisticated concatenation technique (such as that described in Section IV-A) is to reduce the value of u_m . If the concatenation technique succeeds in doing this, then the statistical uncertainty of y_{mer} will be less than that of y_{ave} .

If we ignore error sources that contribute to fluctuations in both y_{ave} and y_{mer} (generally represented by the covariance term $u_{y_{\text{ave}}y_{\text{mer}}}$), then the variance of $y_{\text{ave}} - y_{\text{mer}}$ can be modeled as:

$$u_{y_{\text{ave}}-y_{\text{mer}}}^2 \approx u_{y_{\text{ave}}}^2 + u_{y_{\text{mer}}}^2, \quad (12)$$

which, applying (6) and (11), yields:

$$u_{y_{\text{ave}}-y_{\text{mer}}}^2 = \frac{2[N+1]u_x^2 + [N-1]u_m^2}{[N\tau_0]^2}. \quad (13)$$

It is possible for a frequency bias to develop between the two methods, i.e., for the mean value of $y_{\text{ave}} - y_{\text{mer}}$ to differ from zero. Combining (5), (7), and (9) yields:

$$y_{\text{ave}} - y_{\text{mer}} = \frac{\sum_{j=1}^{N-1} [m_j - (x_{j+1,1} - x_{j,N_{\text{es}}})]}{N\tau_0}. \quad (14)$$

Thus, in order for $y_{\text{ave}} - y_{\text{mer}}$ to equal zero, the average value of the estimated discontinuities m_j must be equal to the average of the differences between the first time-transfer estimate of each batch and the last time-transfer estimate of the batch preceding it. (We shall sometimes refer to these latter quantities as the raw discontinuities.)

In a real-life data set, we can discern whether a frequency bias exists between y_{ave} and y_{mer} by comparing the root mean square (RMS) and standard deviation (STDEV) of $y_{\text{ave}} - y_{\text{mer}}$, because:

$$\begin{aligned} \{\text{RMS}(y_{\text{ave}} - y_{\text{mer}})\}^2 &\equiv \frac{\sum_{j=1}^{N_{\text{samp}}} (y_{\text{ave}} - y_{\text{mer}})^2}{N_{\text{samp}}} = \\ \{\text{STDEV}(y_{\text{ave}} - y_{\text{mer}})\}^2 &+ \{\text{mean}(y_{\text{ave}} - y_{\text{mer}})\}^2, \end{aligned} \quad (15)$$

where N_{samp} represents the number of time intervals for which we have estimates of both y_{ave} and y_{mer} . Note that $\text{STDEV}(y_{\text{ave}} - y_{\text{mer}})$ represents the observed fluctuations in $y_{\text{ave}} - y_{\text{mer}}$, whereas $u_{y_{\text{ave}}-y_{\text{mer}}}$ [(12) and (13)] represents the fluctuations in $y_{\text{ave}} - y_{\text{mer}}$ that one would predict based on estimated values of u_m and u_x .

If a frequency bias does exist between y_{ave} and y_{mer} , it is unwise to compare (6) and (11) in order to discern which of the methods yields a smaller uncertainty. That is because $y_{\text{ave}} \neq y_{\text{mer}}$ implies that (6), (11), or both do not adequately represent the uncertainty of the frequency estimate.

It is important to distinguish between equivalence of the methods ($y_{\text{ave}} - y_{\text{mer}} = 0$) and the accuracy of either

one. For example, consider a systematic-error situation in which the endpoints of each batch get “bent” in such a way as to produce a daily frequency error δy . If we choose a concatenation technique in which we merely align the first time-transfer estimate of one batch with the last time-transfer estimate of the previous batch ($m_j = x_{j+1,1} - x_{j, N_{es}}$), then $y_{ave} - y_{mer}$ will be zero, but both methods will be in error by δy .

III. DATA COLLECTION AND ANALYSIS

The GPSCPTT and TWSTFT measurements are recorded at NIST and PTB on an ongoing basis. Measurements collected during MJDs 52926-46 and 53000-17² were analyzed for this experiment. These periods were chosen because the frequency of the PTB fountain CSF1 was measured relative to a local hydrogen maser (i.e., was evaluated) during MJDs 52929-44 and 52999-53014.

The hydrogen masers used in the CSF1 evaluations also were used to drive the GPSCPTT and TWSTFT systems at PTB. The maser used at PTB during MJDs 52926-46 is called H2 and the maser used during MJDs 53000-17 is called H4. We shall refer to both of these masers as HM unless we need to discuss either one in particular. NIST’s realization of Coordinated Universal Time, UTC(NIST), is electronically manifested by a phase microstepper that uses a hydrogen maser as its local oscillator. The output of this phase microstepper (and hence UTC(NIST)) was used to drive both the GPSCPTT and TWSTFT systems at NIST. The frequency values obtained from GPSCPTT can be directly compared to those obtained from TWSTFT because the same clocks provided the references for both systems.

The TWSTFT measurements were made between NIST and PTB several days per week at $\sim 14:50$ UTC using transmit and receive frequencies of 14.3 and 11.5 GHz, respectively. The measurements were performed using the transponder of an INTELSAT geostationary satellite. During MJDs 52926-46, measurements were taken once per day Monday through Friday. During MJDs 53000-17, the intention was to collect TWSTFT measurements once per day 7 days per week; however, equipment failure prevented data collection on MJDs 53003-7 as well as on MJD 53014. At each station, the 1 s data from each measurement session (120 s duration) were fit with a quadratic equation. The midpoints of these fits were used to compute the time-transfer estimate HM-UTC(NIST). This data-reduction procedure is in accordance with the recommendations of the International Telecommunication Union [10].

The GPSCPTT data were collected continuously using dual-frequency geodetic-type receivers and choke-ring antennae. The GPS measurements from all satellites in view were recorded every 30 s on both the L1 (1575 MHz) and L2 (1228 MHz) carrier frequencies. In order to facili-

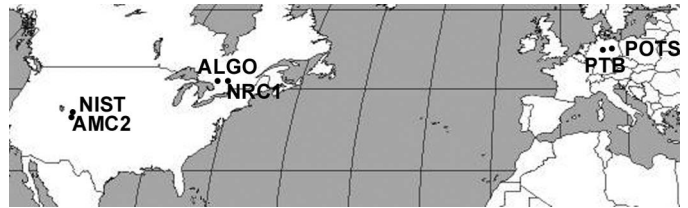


Fig. 1. GPS stations used in computing the GPSCPTT results.

TABLE I
GPS RECEIVER AND DATA TYPES. ALL RECEIVERS USED
AOAD/M.T ANTENNAE.

Site	Receiver	Data types recorded	Notes
NIST	AOA SNR 8000	C1, P2', L1, L2	A, B
PTB	AOA SNR 8000	C1, P2', L1, L2	A, C
ALGO	AOA Benchmark ACT	C1, P1, P2, L1, L2	
AMC2	Ashtech Z-XII3T	C1, P1, P2, L1, L2	
NRC1	AOA SNR-12 ACT, AOA Benchmark ACT	C1, P1, P2, L1, L2	D
POTS	AOA SNR 8000 ACT	C1, P1, P2, L1, L2	

^AP2' \equiv C1 + (P2-P1); the program cc2noncc was used to bring the C1 and P2' data of these receivers into compatibility with the IGS standard. The source code for cc2noncc, as well as the accompanying table of C1-P1 biases, p1c1bias.hist, can be obtained from <https://goby.nrl.navy.mil/IGStime/cc2noncc/cc2noncc.f> and <https://goby.nrl.navy.mil/IGStime/cc2noncc/p1c1bias.hist>.

^BNot the same receiver/benchmark as the IGS station “NISU,” which did not exist at the time these data were taken.

^CNot the same receiver/receiver clock/benchmark as the IGS station “PTBB.”

^DAOA SNR-12 ACT used during MJDs 52926-46; AOA Benchmark ACT used during MJDs 53000-17.

tate ambiguity resolution [11]—a technique that has been shown to improve GPSCPTT results [2]—GPS measurements recorded at the International GNSS Service³ (IGS) stations ALGO (Algonquin Park, Canada), AMC2 (Colorado Springs, CO), NRC1 (Ottawa, Canada), and POTS (Potsdam, Germany) were added to the analysis. As Fig. 1 shows, adding these IGS sites creates three pairs of short baselines (NIST-AMC2, ALGO-NRC1, and PTB-POTS) on which ambiguities can be resolved easily due to the high amount of common satellite visibility (ambiguity resolution depends on having two satellites observed simultaneously at two stations). Once ambiguities are fixed on short baselines, it becomes easier to resolve ambiguities on longer baselines. Adding ALGO and NRC1 bridges the large distance between NIST and PTB, over which there is very little common satellite visibility.

Like NIST and PTB, the IGS sites were equipped with dual-frequency, geodetic-type receivers and choke-ring antennae. Table I provides more information about each site’s receiver and antenna, as well as the data types recorded there.

²October 14–November 3, 2003, and December 27, 2003–January 13, 2004, respectively.

³Formerly known as the International GPS Service.

The data were analyzed in 24-h batches using GIPSY⁴ software provided by the Jet Propulsion Laboratory [12]. Each batch ran from 14:00–13:55 GPST (GPST) to facilitate comparison with the TWSTFT results. In order to concatenate consecutive batches as described in Section IV-A, the data were analyzed a second time in batches that started at 2:00 GPST. Ephemerides for the GPS satellites were obtained from the IGS⁵; earth-orientation parameters were obtained from ⁶. The delay through the ionosphere was removed by forming the “ionosphere-free” linear combination of the L1 and L2 data [13].

UTC(NIST) was chosen to be the reference clock for the GPSCPTT estimates. One value of HM–UTC(NIST) was estimated from each 5 minutes of data; therefore, each 24-h batch of data yielded 288 time-transfer estimates. Both carrier-phase and pseudorange measurements were used during the estimation procedure, with the pseudorange measurements having a weight of 10^{-4} times that of the carrier-phase measurements. The coordinates of the NIST and PTB receiver antennae were estimated as constants over each 24-h batch; the antenna coordinates of the IGS receivers were fixed to the “SINEX” values provided in the IGS’ weekly reference frame products⁵. Other parameters such as zenith troposphere delay were estimated using techniques described in [14].

Although we expect discontinuities between batches of time-transfer estimates, discontinuities also can occur within a batch if a receiver loses lock on all of the satellites at once. Such mid-batch discontinuities, if overlooked, will cause an error in the computation of the frequency. All batches were inspected visually for mid-batch discontinuities; none were found except for on MJDs 52942–43, as discussed in Section VI.

IV. COMPUTING FREQUENCY FROM THE GPSCPTT AND TWSTFT RESULTS

In this method, consecutive sets of time-transfer estimates are concatenated to form a single, continuous time series. The frequency then is computed from this time series. The concatenation is performed as described below

⁴A specific trade name is used for identification purposes only; no endorsement is implied.

⁵Satellite ephemerides: see http://igscb.jpl.nasa.gov/components/prods_cb.html. “Final” orbits from GPS weeks 1240–1243 and 1250–1253 were used. IGS “SINEX” coordinates: see <http://igscb.jpl.nasa.gov/components/prods.html>, heading “Geocentric Coordinates of IGS Tracking Stations (> 130 sites)/Final positions.” Click on one of the analysis-center links (CDDIS, SOPAC, or IGS), then choose “IGS weekly Reference Frame products/Station Positions.” Coordinates for the same weeks as above were used.

⁶See <http://hpiers.obspm.fr/eop-pc/products/bulletins/bulletins.html>; bulletins <ftp://hpiers.obspm.fr/iers/bul/bulb/bulletinb.190>, .191, .192, and .193 were used.

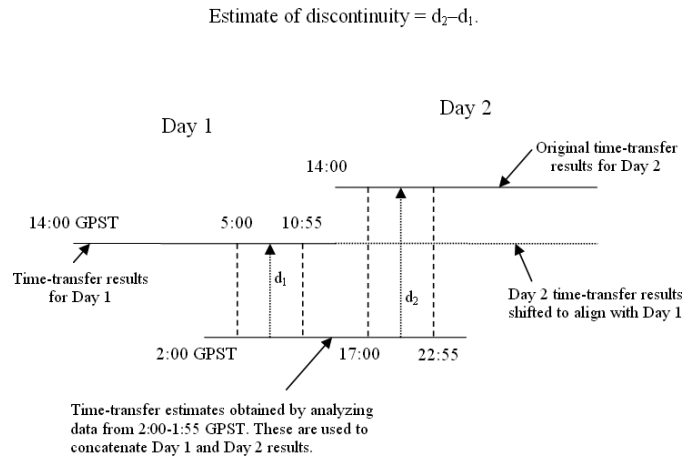


Fig. 2. Method used to concatenate consecutive sets of time-transfer estimates. The solid lines represent sets of time-transfer estimates obtained from 24-h batches of GPS processing. The two sets to be concatenated start at 14:00 GPST. A “transfer” batch is run from 2:00–1:55 GPST in order to connect the sets starting at 14:00. d_1 is computed by subtracting the time-transfer estimates obtained from the 2:00 batch from those obtained from the day 1 batch over the interval 5:00–10:55 GPST, then computing the mean of the differences. d_2 is computed by subtracting the time-transfer estimates obtained from the 2:00 batch from those obtained from the day 2 batch over the interval 17:00–22:55 GPST, then computing the mean of the differences. The day 2 values are shifted by the quantity $d_2 - d_1$. This process is repeated forward through the entire data set.

and as is shown in Fig. 2. For the remainder of this paper, we shall refer to this as the GPSmer method.

Consider consecutive 24-h sets of time-transfer estimates that start at 14:00 GPST, referred to as day 1 and day 2. The discontinuity in time-transfer estimates occurs between the end of the first set (13:55) and the beginning of the next (14:00). To estimate the size of the discontinuity—and thus remove it—a third 24-h set of GPS data that starts at 2:00 GPST is used. This third time series straddles the discontinuity between day 1 and day 2 and provides a continuous set of time-transfer estimates across it.

During the periods over which the day 1 data set overlaps the transfer batch, the difference between the two sets of time-transfer estimates is assumed to be constant—an expectation examined further in Section V. We label this difference as d_1 . The same assumption is made about the difference between the time-transfer estimates of the day 2 batch and the transfer batch, a difference labeled d_2 . The discontinuity between the day 1 and day 2 batches is estimated as $d_2 - d_1$.

d_1 is computed by subtracting the time-transfer estimates obtained from the transfer batch (starts at 2:00 GPST) from those obtained from the day 1 batch over the interval 5:00–10:55 GPST, then computing the mean of these 72 values. d_2 is computed similarly, using the data of the day 2 and transfer batches over the interval 17:00–22:55 GPST. We use difference values from the center of the overlapped periods because the difference values tend to be more constant toward the center and to exhibit greater variability toward the edges.

Once the value of $d_2 - d_1$ is obtained, the time-transfer estimates of day 2 are shifted by the appropriate amount. This process is repeated forward through the data set until all of the batches have been concatenated into a continuous series. The frequency then is computed using (2), but with a slight modification.

The GPS time-transfer estimates are separated by 5-minute intervals. However, as we will show in Section VI and Fig. 5, the time stability of the time-transfer estimates (as measured by the “time deviation” statistic $\sigma_x(\tau)$ [15]) is slightly smaller at $\tau = 10$ minutes than it is at $\tau = 5$ minutes. This implies that averaging two adjacent (separated by 5 minutes) time-transfer estimates will create an estimate that has a smaller uncertainty than either of the two used to create it. Therefore, to compute the mean frequency over a period of interest, the two time-transfer estimates at the beginning of the period are averaged to form one endpoint, as are the two time-transfer estimates at the end of the period. These “averaged” endpoints then are subtracted and divided by the interval between them in order to obtain the frequency.

In GPSSave, the new technique, the GPSCPTT data are processed using GIPSY as described in Section III. However, the discontinuous sets of time-transfer estimates are not concatenated. Rather, a frequency is computed from each set that starts at 14:00 GPST by averaging the first two time-transfer estimates of the set to form one endpoint, the last two time-transfer estimates of the set to form another endpoint, subtracting these averaged endpoints, then dividing by the duration of the interval between them. The mean value of $y(\text{HM-UTC(NIST)})$ for a multiday period then is computed using (7), i.e., by averaging the frequency values that lie within the period of interest.

We are using the first and last two time-transfer estimates of each (14:00 GPST) batch to compute the average frequency for that 24 h. If the time-transfer estimates toward the edges of the batch are corrupted by filter transients, the accuracy of the computed frequency may be compromised. If this proves to be a problem, one can compute the frequency from each batch using some other method (e.g., a linear least-squares fit to the time-transfer values), then average the 24-h frequency values lying within the period of interest as before.

The mean frequency of HM-UTC(NIST) over a multiday period is computed by subtracting the time-transfer estimate at the beginning of the period from the time-transfer estimate at the end of the period and dividing this difference by the interval between the two estimates.

V. PROBLEMS IN ESTIMATING m AND u_m

Consider the values of d_1 and d_2 used in the GPSmer method (Fig. 2). Let:

$$m = d_2 - d_1, \quad (16)$$

represent the estimated value of the discontinuity. Then:

$$u_m^2 \approx u_{d_1}^2 + u_{d_2}^2. \quad (17)$$

Two problems arise in estimating u_{d_1} and u_{d_2} which arise from the overlap difference values averaged to compute d_1 and d_2 . The problems are as follows. (We shall discuss the computation of d_1 and u_{d_1} with the understanding that the same problems apply to the computation of d_2 and u_{d_2} .)

The first problem is, the difference values averaged to obtain d_1 may exhibit correlated noise rather than white phase noise. Fig. 3(a) shows an example. If the noise were white, we could use the uncertainty of the mean (expressed as $\text{STDEV}(\text{difference values})/\sqrt{72}$) as an estimator for u_{d_1} . However, if the noise is not white, then this is not appropriate.

The second problem in estimating d_1 is that the difference values averaged to obtain it may not exhibit a slope of zero, i.e., they may not converge toward some central value over the 5 h, 55 minute averaging period. [Figs. 3(b)–(c) show some of the worst examples from our data.] In this case, using the average of these values may produce a biased estimate of d_1 , which adds an unknown quantity to u_{d_1} .

The first problem is more common in our results than the second problem. Both problems indicate that, over the period 5:00–10:55 GPST (or 17:00–22:55 GPST), the time-transfer estimates in the “primary” 14:00–13:55 batch are correlated to each other in a way that is different from the way in which the time-transfer estimates of the 2:00–1:55 “transfer” batch are correlated to each other. This, in turn, implies that, even if it is at a low level, $u_{x_{j,s}x_{j,t}} \neq 0$.

To put the second problem in perspective, it may be that the net slope in the difference values averaged to obtain d_1 is small compared to the size of the day-boundary discontinuity. For example, in a bad case, the difference values averaged to compute d_1 may exhibit a net change of 40 ps over the course of 5 h, 55 minutes, whereas the day-boundary discontinuity being estimated and removed may be on the order of several hundred picoseconds. In this case, the frequency error introduced by misestimating d_1 (i.e., the addition to u_m) will be small compared with the frequency error incurred by not removing the day-boundary discontinuity and computing a frequency across it.

In this study, we estimated u_{d_1} by computing the standard deviation of the difference values averaged to compute d_1 (as opposed to $\text{STDEV}(\text{difference values})/\sqrt{72}$). This ad-hoc estimate at least grows larger when there is a nonzero slope in the values averaged to estimate d_1 . u_{d_2} was computed analogously. A superior approach for the

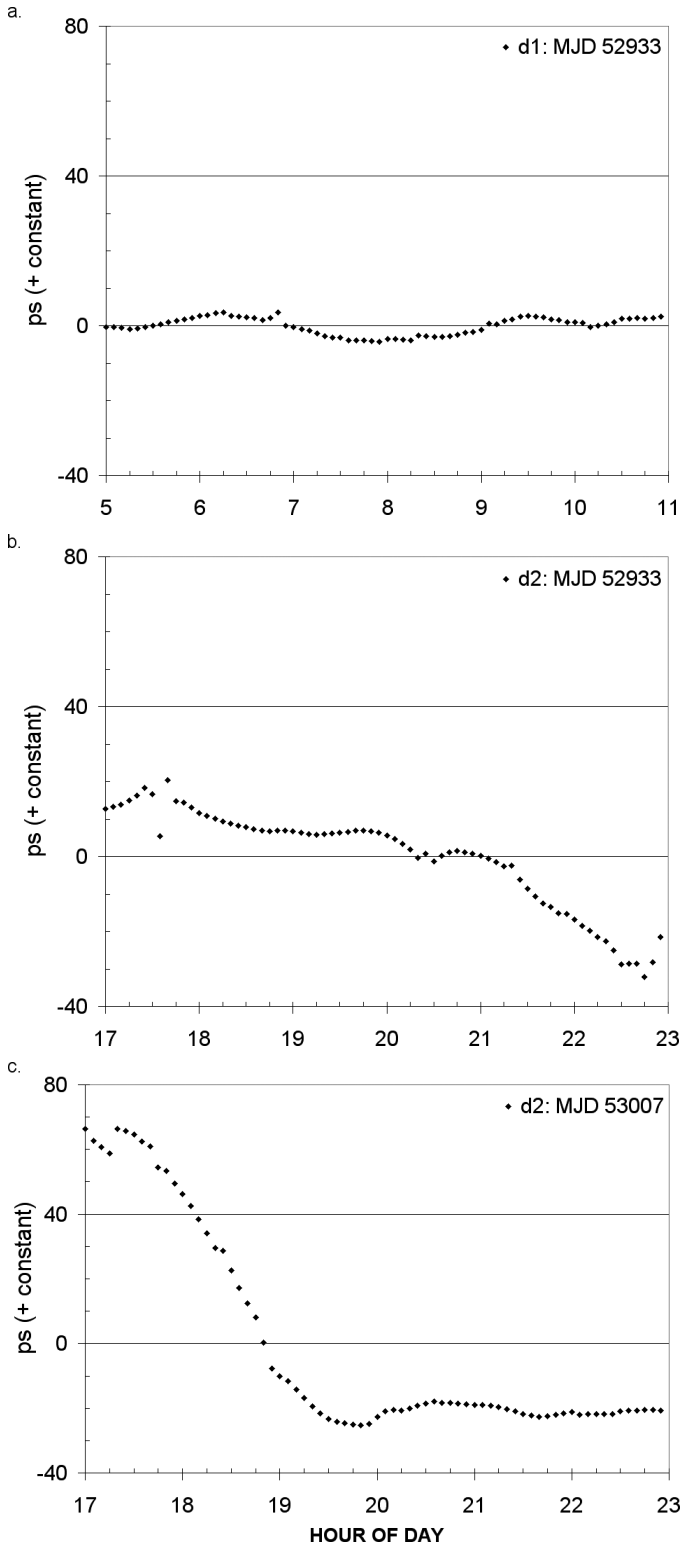


Fig. 3. Examples of the values averaged to compute d_1 and d_2 [see Fig. 2 and (16)]. Constants of 907, 76, and 446 ps were added to the values in (a)–(c), respectively.

future would be to analyze the noise characteristics of the difference values using the $\sigma_x(\tau)$ statistic [15] and to optimize the estimation of d_1 and u_{d_1} based on the results.

u_{d_1} and u_{d_2} are different for each concatenation. We arrive at an overall estimate of u_m using:

$$u_m^2 = \frac{\sum_{k=1}^{N_{\text{cat}}} [u_{d_{k,1}}^2 + u_{d_{k,2}}^2]}{N_{\text{cat}}}, \quad (18)$$

where N_{cat} is the total number of concatenations made in the GPSmer method.

VI. RESULTS AND DISCUSSION

Fig. 4 shows the frequency of the maser at PTB relative to UTC(NIST) as computed from GPSCPTT and TWSTFT. The GPSCPTT values were obtained using the GPSave method. The TWSTFT values were obtained by subtracting adjacent TWSTFT time-transfer estimates and dividing by the interval between them. As Fig. 4 shows, the GPSCPTT and TWSTFT results agree well.

In Fig. 4(a), H2–UTC(NIST) shows a sharp change in frequency of about $1 \cdot 10^{-14}$ at approximately MJD 52934. Using frequency-estimation techniques appropriate to WHFM noise may not be optimal when the mean frequency is computed across intervals containing frequency steps of this magnitude.

As Fig. 4(a) shows, there is a gap in the GPSCPTT values for MJDs 52942–43. The ionosphere was extremely active during this period⁷, causing outages at some of the receivers and rendering the GPSCPTT results so full of jumps as to be nearly unusable. Although GPS results could be obtained once again for MJDs 52944–46 and daily frequencies computed using the GPSave method, we did not concatenate the time-transfer estimates using the GPSmer method past MJD 52941.

Fig. 5 shows the time and frequency stability of the results as measured by $\sigma_x(\tau)$ [15] and by the Allan Deviation $\sigma_y(\tau)$ [7]. The $\sigma_x(\tau)$ plots show that the measurement noise is approximately WHPM at averaging times of 5–10 minutes, and that it, therefore, is appropriate to average adjacent 5-minute time-transfer estimates when creating endpoints. We use $\sigma_x(\tau = 10 \text{ minutes})$ to represent the variable u_x in (6)–(13). As Fig. 5 shows, $\sigma_x(\tau = 10 \text{ minutes})$ is 11 and 12 ps for the two data sets; we will set $u_x = 12 \text{ ps}$ for the remainder of this paper. The $\sigma_y(\tau)$ plots show that the noise type up to $\tau = 1 \text{ d}$ is consistent with WHFM, and that it is appropriate to use a modified version of (9) (as described in Section IV-B) in computing a frequency from each 24-h set of time-transfer estimates.

Figs. 6 and 7 show the RMS difference of the values of $y(\text{HM} - \text{UTC}(\text{NIST}))$ obtained using GPSmer, GPSave, and TWSTFT. The RMS difference is assessed as a func-

⁷<http://www.cx.unibe.ch/aiub/ionosphere.html>; see “Exceptionally high TEC levels on days 302 and 303 of 2003.” See also http://www.aiub.unibe.ch/ionosphere/gim_29-oct-2003.gif, which shows global TEC values for days 301–304, 2003.

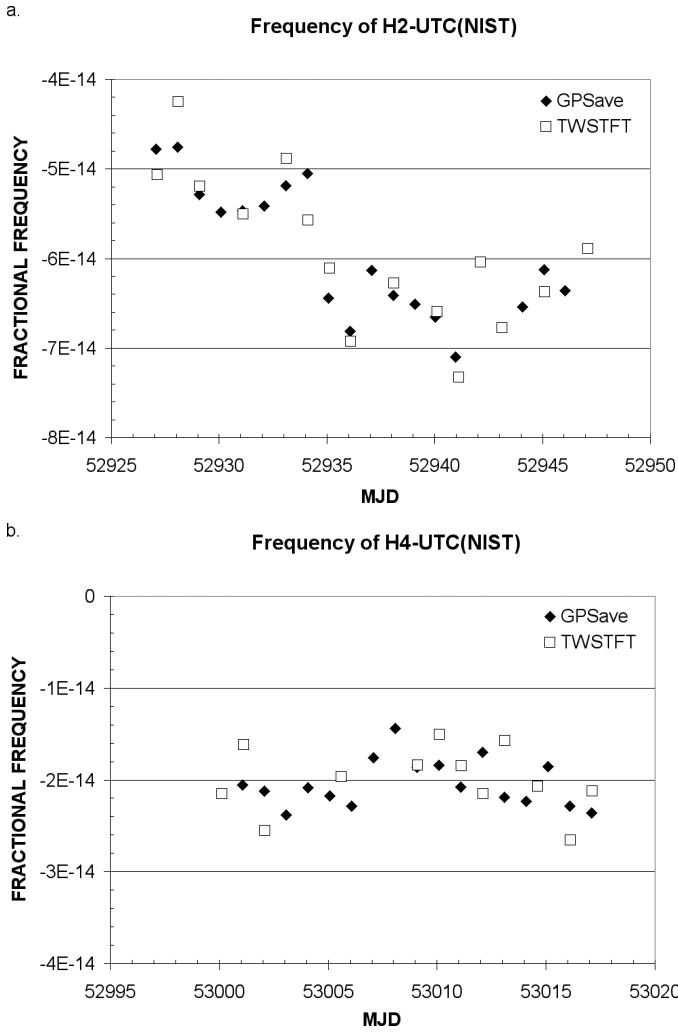


Fig. 4. Fractional frequencies derived from GPSCPTT and TWSTFT. The GPSCPTT values were computed using the GPSave method, i.e., each frequency shown was computed from a single 24-h batch of data. The TWSTFT values were obtained by subtracting adjacent time-transfer values and dividing by the interval between them. As an example, the TWSTFT time-transfer values obtained for epochs 53001.6 and 53002.6 were used to compute a frequency value that is plotted at MJD 53002.1; the GPSCPTT batch that ran from 53001.6 to 53002.6 was used to compute a frequency that is plotted at MJD 53002.1.

tion of averaging time for $\tau \geq 2$ d. The values in the figures were derived as follows.

Suppose we wish to compute the RMS difference of the frequencies derived using TWSTFT and GPSmer for $\tau = 2$ d and MJDs 53000-17. There are seven subsets of TWSTFT data that have an averaging time of 2 d: 53000-02, 53008-10, 53009-11, 53010-12, 53011-13, 53013-15, and 53015-17⁸. We compute $y(\text{H4-UTC(NIST)})$ for each period using TWSTFT and GPSmer, then subtract. For example, for MJDs 53013-15, $y_{\text{TWSTFT}}(\text{H4-UTC(NIST)}) = -20.69 \cdot 10^{-15}$ and $y_{\text{GPSmer}}(\text{H4-UTC(NIST)}) = -19.92 \cdot$

⁸The TWSTFT measurements are taken at approximately 14:50 UTC; therefore, it would be more accurate to refer to these periods as “53000.6 - 53002.6,” etc. This is not done for the sake of brevity.

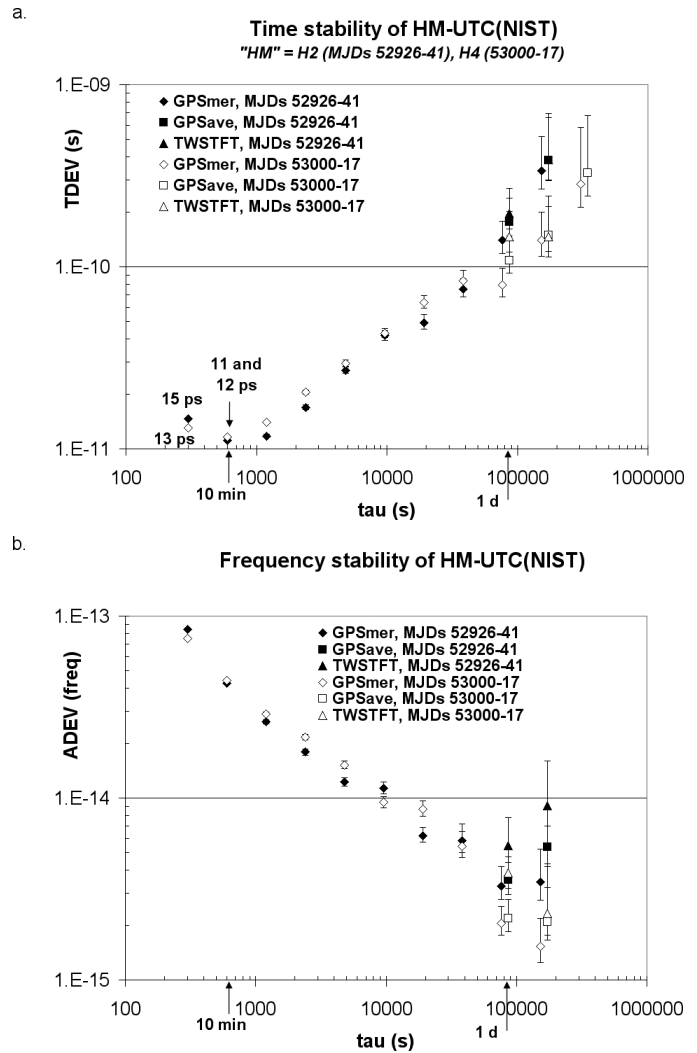


Fig. 5. Time and frequency stability of the GPSCPTT and TWSTFT results. “TDEV” is equal to the time deviation statistic $\sigma_x(\tau)$ [15]. “ADEV” is equal to the Allan deviation $\sigma_y(\tau)$ [7]. The values from MJDs 52926-41 should not be compared directly to the values from MJDs 53000-17, because “HM” was not the same maser in both cases. The stability values for GPSmer were computed from the concatenated time-transfer estimates (which were spaced at 5-minute intervals); stability values for GPSave were computed from daily fractional frequency values (Fig. 4) spaced at 1-d intervals. Stability values for TWSTFT were computed from the TWSTFT-derived time-transfer estimates; these were spaced at integer multiples of 1 d.

10^{-15} . Thus, $y_{\text{GPSmer}} - y_{\text{TWSTFT}} = 0.77 \cdot 10^{-15}$. The above procedure yields seven estimates of $y_{\text{GPSmer}} - y_{\text{TWSTFT}}$ for $\tau = 2$ d and MJDs 53000-17. We save the values with the smallest (“best”) and largest (“worst”) magnitudes to use as error bars on the RMS (computed below).

The RMS difference for $\tau = 2$ d, MJDs 53000-17 then is computed using nonoverlapping samples, i.e., using values of $y_{\text{GPSmer}} - y_{\text{TWSTFT}}$ that have no GPSCPTT or TWSTFT data in common. For example, the values of $y_{\text{GPSmer}} - y_{\text{TWSTFT}}$ for MJDs 53008-10 and 53009-11 both include GPSCPTT time-transfer estimates from MJD 53009-10. Therefore, only one of these values is used

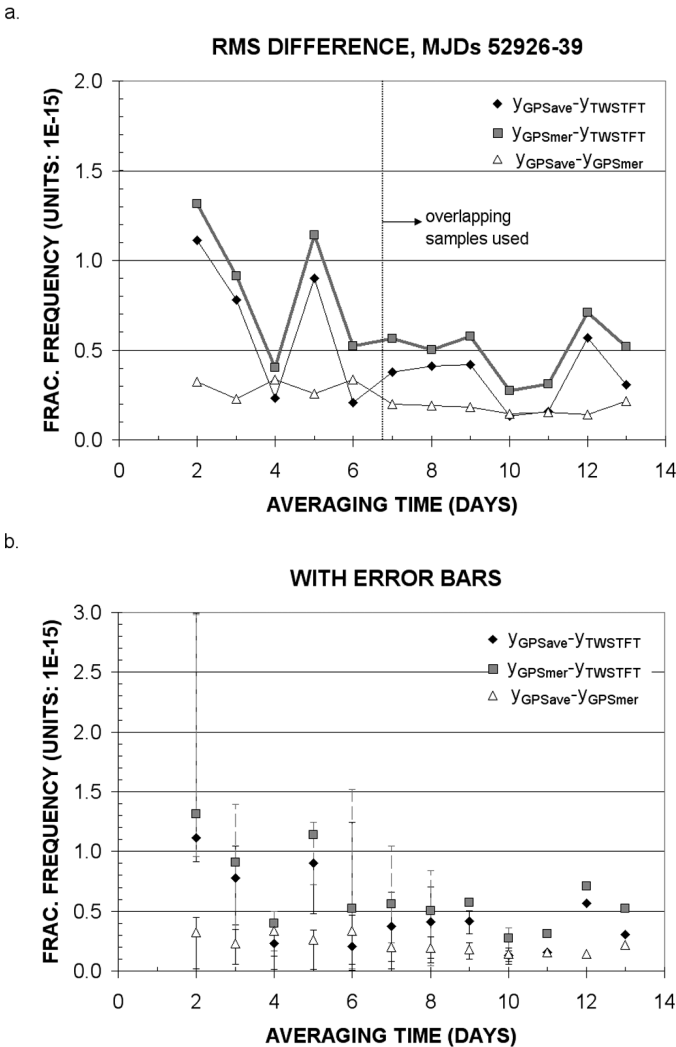


Fig. 6. RMS difference of frequency values obtained from GPSave, GPSmer, and TWSTFT: MJDs 52926-39. Nonoverlapping samples are used in computing the RMS when possible; see text for details. The error bars mark the largest (worst) and smallest (best) difference in values observed between two techniques for a given averaging time. All values, not just nonoverlapping ones, were sampled in finding best and worst. The gray dashed error bars correspond to $y_{GPSmer-y_{TWSTFT}}$; other error bars are shown in solid black.

in computing the RMS. When multiple sets of independent samples are available (e.g., for $\tau = 3$ d, MJDs 53008-11 and 53012-15 or 53008-11 and 53013-16 could be used), we choose the set with the largest average interval between samples.

The above process is repeated within the MJD 53000-17 data set for all possible averaging times and for the quantities $y_{GPSave-y_{TWSTFT}}$ and $y_{GPSave-y_{GPSmer}}$. When the averaging time becomes too large to permit the use of nonoverlapping samples, overlapping samples are used instead. The entire process then is repeated for MJDs 52926-39.

As Figs. 6 and 7 show, GPSCPTT and TWSTFT exhibit good agreement at short averaging times. The evaluation of a cesium fountain frequency standard typically lasts at least 15 d, but the RMS value of $y_{GPSCPTT-y_{TWSTFT}}$

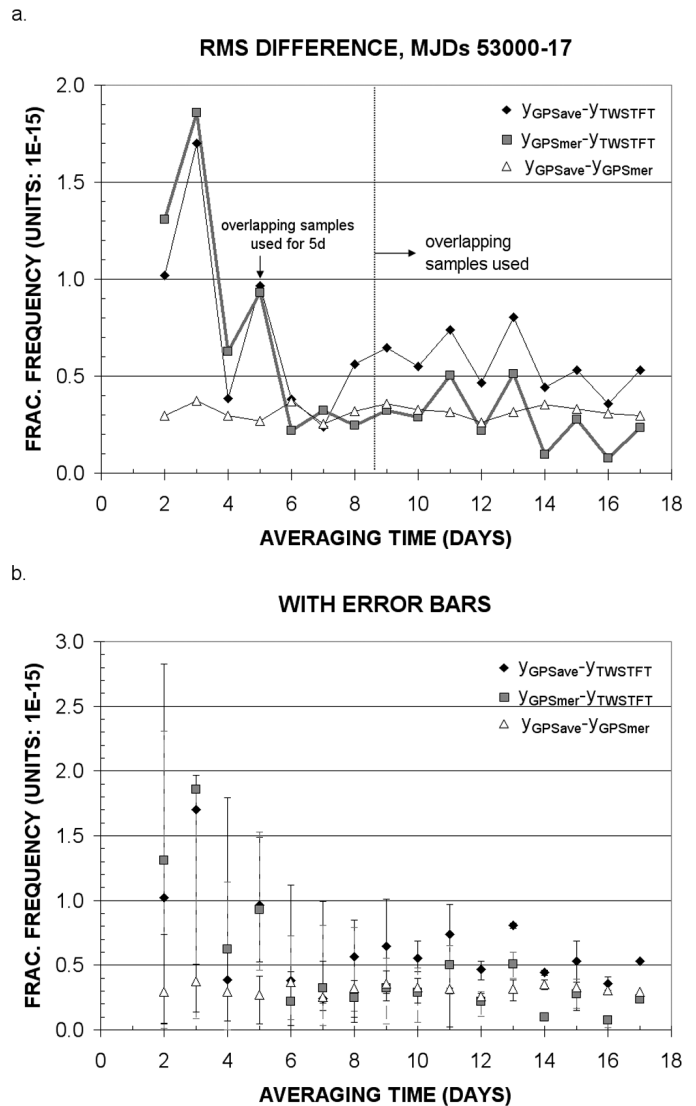


Fig. 7. Same as Fig. 6, but for MJDs 53000-17.

is always smaller than $1 \cdot 10^{-15}$ for $\tau \geq 4$ d regardless of which GPSCPTT technique is used⁹. In fact, for MJDs 52926-39, the RMS value of $y_{GPSCPTT-y_{TWSTFT}}$ is usually in the range of $2 - 6 \cdot 10^{-16}$ for $\tau \geq 4$ d, and the “worst” value never exceeds $1 \cdot 10^{-15}$ once $\tau \geq 8$ d. For MJDs 53000-17, the RMS value of $y_{GPSCPTT-y_{TWSTFT}}$ is usually in the range of $2 - 7 \cdot 10^{-16}$ for $\tau \geq 4$ d, although twice the number gets as high as $8 - 9 \cdot 10^{-16}$. Also, the “worst” value never exceeds $1 \cdot 10^{-15}$ once $\tau \geq 9$ d.

The frequency agreement between GPSCPTT and TWSTFT represents the combined frequency uncertainty of the two methods. The above facts imply that the uncertainties of both GPSCPTT and TWSTFT are small enough that either technique could be considered viable for use during a simultaneous fountain evaluation. These techniques are capable of achieving the level of performance needed for this task in as few as 8 to 9 d.

⁹The exception to this is the RMS value of $y_{GPSmerge-y_{TWSTFT}}$ for $\tau = 5$ d during MJDs 52926-39.

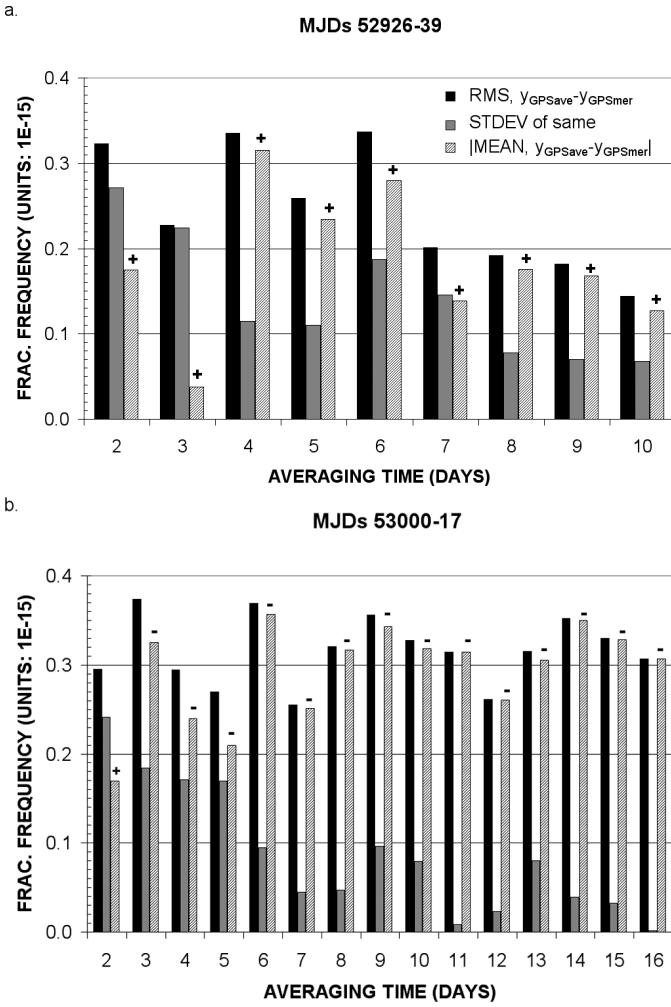


Fig. 8. Computation of bias between y_{GPSsave} and y_{GPSmer} by use of (15). If the methods produced the same frequency values, RMS would equal STDEV. The sign of the computed mean value of $y_{\text{GPSsave}} - y_{\text{GPSmer}}$ is shown above each striped bar; the size of the bar corresponds to its absolute value. $y_{\text{GPSsave}} - y_{\text{GPSmer}}$ is consistently positive for MJDs 52926-39. It is consistently negative for MJDs 53000-17, with the exception of averaging time = 2 d.

Figs. 6 and 7 show that the frequencies derived from the GPSave method agree with those derived from the GPSmer method at $1 - 4 \cdot 10^{-16}$ RMS. If we compute the standard deviation (STDEV) of $y_{\text{GPSsave}} - y_{\text{GPSmer}}$ using the same sampling technique as was used for the RMS, then apply (15), we find that much of the RMS difference between the methods stems from a small frequency bias between them. This is shown in Fig. 8. The absolute value of $\{\text{mean}[y_{\text{GPSsave}} - y_{\text{GPSmer}}]\}$ is $\sim 1 - 3 \cdot 10^{-16}$ for MJDs 52926-39 and $\sim 3 \cdot 10^{-16}$ for MJDs 53000-17, with the effect more pronounced for the latter data set. For MJDs 52926-39, the GPSave method produces a frequency estimate consistently higher than that produced by the GPSmer method. For MJDs 53000-17, the situation is reversed.

Table II shows the u_{d_1} and u_{d_2} values computed for MJDs 52926-39 and 53000-17. Applying (18) yields values of $u_m = 9$ and 21 ps for the two periods, respectively. u_m is larger for MJDs 53000-17 because several of the

TABLE II
ESTIMATING u_m .

A. MJDS 52926-39		
MJD	u_{d_1} , ps (5:00–10:55 GPST)	u_{d_2} , ps (17:00–22:55 GPST)
52927	6	7
52928	4	4
52929	3	2
52930	4	4
52931	4	6
52932	3	6
52933	2	13
52934	4	15
52935	6	7
52936	3	7
52937	10	3
52938	3	3
$u_m = \sqrt{\{\Sigma [u_{d_1}^2 + u_{d_2}^2] / 12\}} = 9$ ps		
B. MJDS 53000-17		
MJD	u_{d_1} , ps (5:00–10:55 GPST)	u_{d_2} , ps (17:00–22:55 GPST)
53001	9	7
53002	13	5
53003	4	17
53004	8	42
53005	13	2
53006	4	3
53007	3	32
53008	7	29
53009	4	8
53010	8	12
53011	7	34
53012	8	4
53013	9	14
53014	14	4
53015	3	18
53016	6	3
$u_m = \sqrt{\{\Sigma [u_{d_1}^2 + u_{d_2}^2] / 16\}} = 21$ ps		

17:00–22:55 GPST overlap sessions used to compute d_2 had nonzero slopes similar to that shown in Fig. 3(c). Mid-batch discontinuities were not observed in either of the sets of time-transfer estimates subtracted to compute d_2 , so it is not clear what the source of the step-like behavior is.

Using the Table II values of u_m as well as $u_x = 12$ ps (Fig. 5), we can generate values of $u_{y_{\text{GPSmer}}}$ and $u_{y_{\text{GPSsave}}}$ from (6) and (11), then compare their quadrature sum, $u_{y_{\text{GPSsave}} - y_{\text{GPSmer}}}$ (12), which represents a predicted value for the fluctuations in $y_{\text{GPSsave}} - y_{\text{GPSmer}}$, to the observed fluctuations in $y_{\text{GPSsave}} - y_{\text{GPSmer}}$ as measured by STDEV. The comparison is shown in Fig. 9. We see that, when using these values of u_m and u_x , $u_{y_{\text{GPSmer}}} < u_{y_{\text{GPSsave}}}$ for MJDs 52926-39 and $u_{y_{\text{GPSsave}}} < u_{y_{\text{GPSmer}}}$ for MJDs 53000-17. (This is what we would expect from (6) and (11).) However, we also see that, at shorter averaging times, $u_{y_{\text{GPSsave}} - y_{\text{GPSmer}}}$ is smaller than $\text{STDEV}(y_{\text{GPSsave}} - y_{\text{GPSmer}})$. This indicates that the values used for u_x and/or u_m may be too small. This fact, along with the existence of the bias between y_{GPSsave} and y_{GPSmer} , implies that, at this stage,

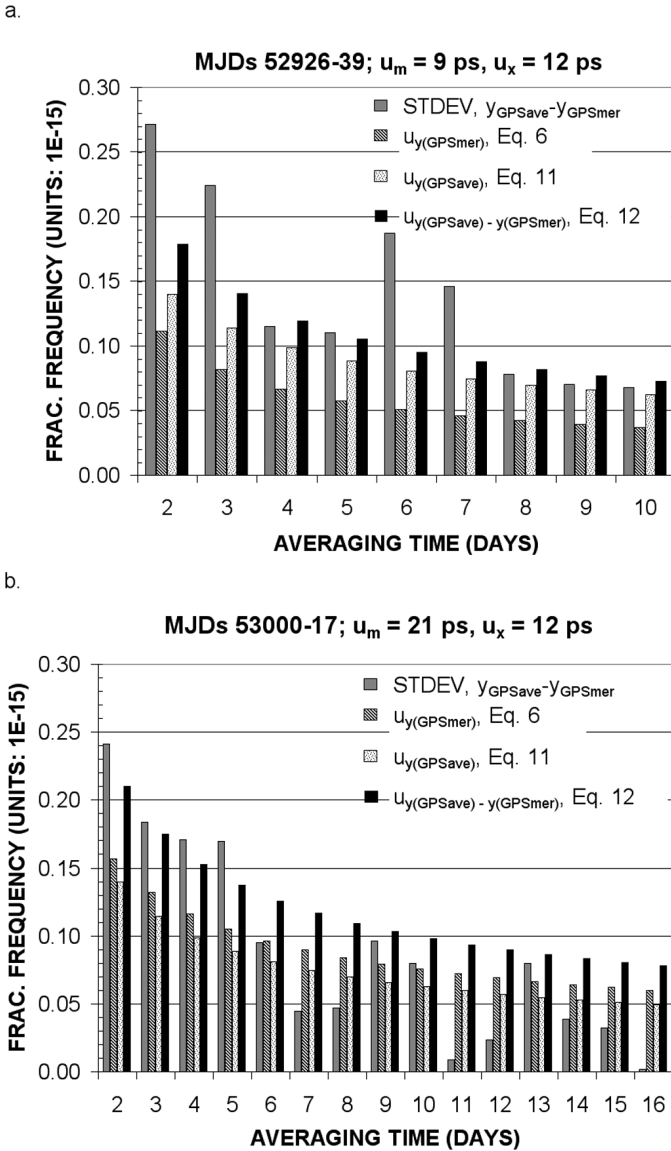


Fig. 9. Observed (STDEV) and predicted ($u_{y_{GPSsave} - y_{GPSmer}}$) fluctuations in $y_{GPSsave} - y_{GPSmer}$. $u_{y_{GPSsave} - y_{GPSmer}}^2 = u_{y_{GPSmer}}^2 + u_{y_{GPSsave}}^2$. If u_x , u_m , (6), (11), and (12) are correct, then $u_{y_{GPSsave} - y_{GPSmer}}$ should be approximately equal to STDEV.

it is difficult to tell whether GPSave or GPSmer produces frequency values with smaller uncertainty.

Eq. (14) showed that there will be a frequency bias between $y_{GPSsave}$ and y_{GPSmer} if the average of the discontinuities estimated in the GPSmer method is either larger or smaller than the average of the raw discontinuities. Fig. 10 compares these values. (Note that, in computing the “raw” discontinuities, we subtract the average of the 13:50 and 13:55 time-transfer estimates from the average of the 14:00 and 14:05 estimates. We also correct the estimated-“raw” discontinuity values by -34 ps [= $(600 \text{ s}) \cdot (-5.7 \cdot 10^{-14})$] and -12 ps [= $(600 \text{ s}) \cdot (-2.0 \cdot 10^{-14})$] for MJDs 52926-39 and 53000-17 to account for the portion of the raw discontinuity caused by the frequency difference of the oscillators accumulating over 10 minutes.) As Fig. 10 shows, the difference between the estimated and raw discontinuities

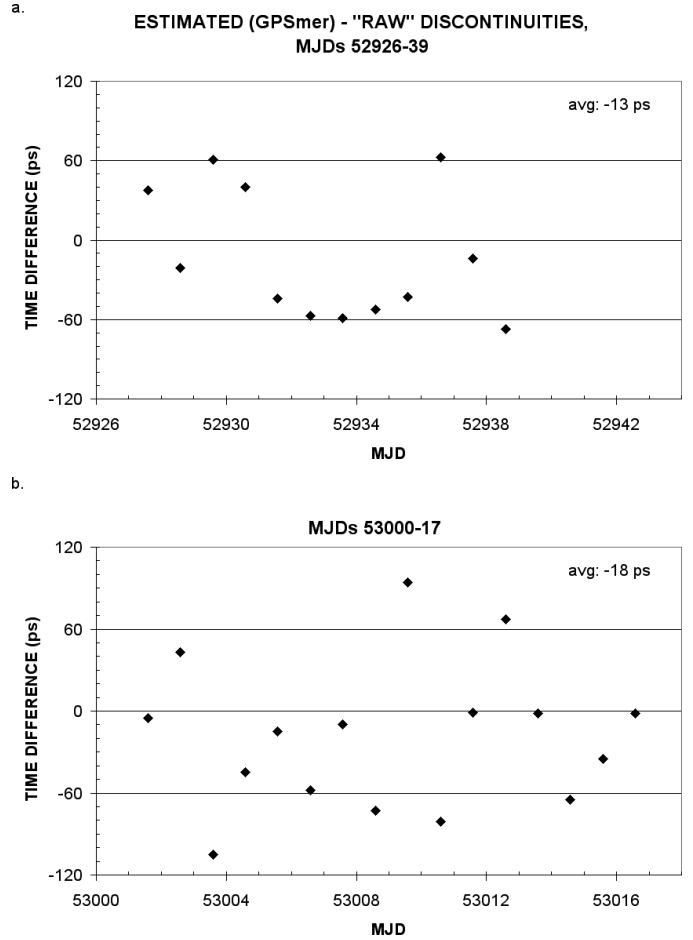


Fig. 10. Difference between day-boundary discontinuities estimated by GPSmer (§IV-A) and “raw” ones computed using $\{\text{average}[x_j(14:00), x_j(14:05)] - \text{average}[x_{j-1}(13:50), x_{j-1}(13:55)]\}$. x_j represents a time-transfer estimate from the j^{th} batch. The discontinuity-difference values plotted in (a) and (b) have been adjusted by -34 ps and -12 ps, respectively; see text for details.

tends to be negative for MJDs 53000-17, which is consistent with the negative bias shown in Fig. 8. The situation is less clear for MJDs 52926-39. Although there are some strongly positive values, the overall average is slightly negative. Further investigation is needed to see if there indeed is a bias between $y_{GPSsave}$ and y_{GPSmer} and, if so, what causes it.

As stated previously, the PTB fountain CSF1 was evaluated during MJDs 52929-44 and 52999-53014. Therefore, it is possible to compute the frequency $y(\text{CSF1-UTC}(\text{NIST}))$ for these periods using the GPSCPTT and TWSTFT results of this paper, then to compare these values to those that can be obtained from

¹⁰. This provides an additional check of the GPSCPTT results. It does not provide an independent check of the TWSTFT results because the BIPM uses NIST-PTB TWSTFT measurements in computing UTC. However, it is interesting to see how well the TWSTFT and GPSCPTT frequency estimates agree for the periods in question.

¹⁰BIPM Circular T 190-193; [ftp://62.161.69.5/pub/tai/publication/cirt.190, 191, 192, 193](ftp://62.161.69.5/pub/tai/publication/cirt.190,191,192,193).

TABLE III
ESTIMATING $y(\text{CSF1-UTC}(\text{NIST}))$ FROM *BIPM Circular T*.

MJD	$y(\text{CSF1-UTC})^A$	$y(\text{UTC-UTC}(\text{NIST}))^B$	$y(\text{CSF1-UTC}(\text{NIST}))$
units: 10^{-15}			
52929-39	11.0 ^C	0.5	11.5
52999-53014	13.2	0.2	13.4

^AScale interval “d” reported by BIPM in §4 of *Circular T*¹⁰.

^BComputed from time series UTC-UTC(NIST) published in §1 of *Circular T*¹⁰.

^CWe needed a value for MJDs 52929-39 rather than 52929-44; therefore, $y(\text{CSF1-UTC})$ could not be obtained from §4 of *Circular T*¹⁰. It was obtained from [16], [17] instead.

$y(\text{CSF1-UTC}(\text{NIST}))$ was computed from the GPSCPTT and TWSTFT results of this paper using

$$y(\text{CSF1-UTC}(\text{NIST})) = y(\text{CSF1-HM}) + y(\text{HM-UTC}(\text{NIST})). \quad (19)$$

The first quantity on the right-hand side was measured by PTB during each fountain evaluation. The second quantity is the frequency obtained from GPSCPTT or TWSTFT.

$y(\text{CSF1-UTC}(\text{NIST}))$ was computed from ¹⁰ using the equation:

$$y(\text{CSF1-UTC}(\text{NIST})) = y(\text{CSF1-UTC}) + y(\text{UTC-UTC}(\text{NIST})). \quad (20)$$

$y(\text{CSF1-UTC})$ is equal to the scale interval d reported in Section 4 of ¹⁰. $y(\text{UTC-UTC}(\text{NIST}))$ was computed from Section 1 of ¹⁰ by subtracting the values of UTC-UTC(NIST) corresponding to the endpoints of the period of interest.

Table III shows the $y(\text{CSF1-UTC}(\text{NIST}))$ estimates obtained from ¹⁰ [via (20)] for MJDs 52929-39 and 52999-53014. (We used 52929-39 rather than 52929-44 because the time-transfer estimates could not be concatenated past 52941.) The values of $y(\text{CSF1-UTC})$ (i.e., d) have uncertainties of approximately $2.5 \cdot 10^{-15}$ ¹⁰. Therefore, the values of $y(\text{CSF1-UTC}(\text{NIST}))$ derived from ¹⁰ will have uncertainties greater than or equal to this.

Table IV shows how well the values of $y(\text{CSF1-UTC}(\text{NIST}))$ computed from GPSCPTT, TWSTFT, and ¹⁰ agree. For MJDs 52929-39, the GPSCPTT-based values agree with those obtained from ¹⁰ at $3 - 4 \cdot 10^{-16}$, well within the $2.5 \cdot 10^{-15}$ uncertainty stated above. The GPSCPTT and TWSTFT frequency estimates agree among themselves at $3 \cdot 10^{-16}$. In contrast, over the interval MJD 52999-53014, the GPSCPTT values showed some of the worst agreement with TWSTFT of this entire experiment: the GPSCPTT/TWSTFT frequency values have a spread of $0.8 \cdot 10^{-15}$. Nonetheless, the GPSCPTT-based values of $y(\text{CSF1-UTC}(\text{NIST}))$ are within $1.8 \cdot 10^{-15}$ of the ¹⁰ value.

VII. CONCLUSIONS

A new technique for computing frequency from GPS carrier-phase time-transfer estimates is proposed and tested. This new technique circumvents the discontinuities that appear in time-transfer estimates between the end of one processing batch and the beginning of the next. An approach often used in the past has been to concatenate the time-transfer estimates by estimating and removing the discontinuities. The frequency then is computed from the continuous time series. In the new technique, a frequency value is first computed directly from each set of time-transfer estimates. The mean frequency over a multi-day period then is computed by simply averaging (or otherwise combining) the individual frequency values lying within that period.

The new technique was tested by comparing the frequency values it yields with those obtained using a concatenation technique and those obtained using TWSTFT. The frequency values obtained from the GPSCPTT measurements using the new technique agreed with those obtained using the concatenation technique at $1 - 4 \cdot 10^{-16}$ RMS. Part of that number arose from a frequency bias between the methods. We do not know the source of the bias; therefore, it is difficult to say which of the methods offers smaller uncertainty. The frequency values obtained from the GPSCPTT data using either of the two techniques agreed with those obtained from the TWSTFT data at several parts in 10^{16} for averaging times of 4 d or greater. One would expect little common-mode error cancellation between GPSCPTT and TWSTFT; therefore, this implies that both GPSCPTT and TWSTFT are approaching a level of frequency-transfer performance sufficient for use during simultaneous fountain evaluations.

ACKNOWLEDGMENTS

The authors thank Andreas Bauch (PTB), Jim Ray (National Geodetic Survey), Marc Weiss (NIST), Victor Zhang (NIST), and the reviewers at ¹⁰ for comments regarding the manuscript. They also thank Gérard Petit of the Bureau International des Poids et Mesures and Stefan Weyers of PTB for providing estimates of $y(\text{CSF1-UTC})$ and $y(\text{CSF1-HM})$.

REFERENCES

- [1] K. M. Larson, J. Levine, L. M. Nelson, and T. E. Parker, “Assessment of GPS carrier-phase stability for time-transfer applications,” *IEEE Trans. Ultrason., Ferroelect., Freq. Contr.*, vol. 47, pp. 484–494, 2000.
- [2] R. Dach, G. Beutler, U. Hugentobler, S. Schaer, T. Schildknecht, T. Springer, G. Dudle, and L. Prost, “Time transfer using GPS carrier phase: Error propagation and results,” *J. Geodesy*, vol. 77, pp. 1–14, 2003.
- [3] A. Bauch, R. Dach, J. Davis, L. Lorini, T. Parker, G. Petit, and J. Richard, “Time and frequency comparisons between four European timing institutes and NIST using multiple techniques,” in *Proc. 19th Eur. Time Freq. Forum*, 2005.

TABLE IV
COMPARISON OF GPSCPTT/TWSTFT ESTIMATES OF $Y(\text{CSF1-UTC}(\text{NIST}))$ WITH VALUES OBTAINED FROM *BIPM Circular T*.

$y(\text{CSF1-HM}) = 69.6 \cdot 10^{-15}$ for MJDs 52929-39 ^A (add this to column 3 to obtain column 4)				
Method	Averaging epoch	$y(\text{HM-UTC}(\text{NIST}))$	$y(\text{CSF1-UTC}(\text{NIST}))$	$y_{\text{method-}}^{\text{Circular T}}$ (cf Table III)
units: 10^{-15}				
TWSTFT	52928.6-	-58.2	11.4	-0.1
GPSave	52939.6	-58.4	11.2	-0.3
GPSmer		-58.5	11.1	-0.4
$y(\text{CSF1-HM}) = 31.6 \cdot 10^{-15}$ for MJDs 52999-53014 ^A				
TWSTFT	53000.6-	-19.2	12.4	-1.0
GPSave	53013.6	-20.0	11.6	-1.8
GPSmer		-19.8	11.8	-1.6

^AMeasured by PTB during fountain evaluation [16].

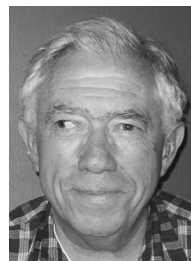
- [4] J. Ray and K. Senior, "IGS/BIPM pilot project: GPS carrier phase for time/frequency transfer and timescale formation," *Metrologia*, vol. 40, pp. S270-S288, 2003.
- [5] R. Dach, T. Schildknecht, U. Hugentobler, L.-G. Bernier, and G. Duddle, "Continuous geodetic time transfer analysis method," *IEEE Trans. Ultrason., Ferroelect., Freq. Contr.*, vol. 53, no. 7, pp. 1250-1259, 2006.
- [6] K. Senior, E. Powers, and D. Matsakis, "Attenuating day-boundary discontinuities in GPS carrier-phase time transfer," in *Proc. 31st Annu. Precise Time Interval Meeting*, 1999, pp. 481-490.
- [7] D. W. Allan, "Time and frequency (time-domain) characterization, estimation, and prediction of precision clocks and oscillators," *IEEE Trans. Ultrason., Ferroelect., Freq. Contr.*, vol. UFFC-34, pp. 647-654, 1987.
- [8] T. E. Parker, "Hydrogen maser ensemble performance and characterization of frequency standards," in *Proc. Joint Meeting Eur. Freq. Time Forum and IEEE Int. Freq. Contr. Symp.*, 1999, pp. 173-176.
- [9] J. A. Kusters, L. S. Cutler, and E. D. Powers, "Long-term experience with cesium beam frequency standards," in *Proc. Joint Meeting Eur. Freq. Time Forum and IEEE Int. Freq. Contr. Symp.*, 1999, pp. 159-163.
- [10] International Telecommunication Union, "The operational use of two-way satellite time and frequency transfer employing PN time codes," in *ITU-R TF.1153-2*. Geneva, Switzerland: International Telecommunication Union, 2003.
- [11] G. Blewitt, "Carrier-phase ambiguity resolution for the Global Positioning System applied to geodetic baselines up to 2000 km," *J. Geophys. Res.*, vol. B94, pp. 10,187-10,203, 1989.
- [12] F. H. Webb and J. F. Zumberge, Eds. *An Introduction to GIPSY/OASIS-II: Precision Software for the Analysis of Data from the Global Positioning System*. Pasadena, CA: Jet Propulsion Laboratory, Jun. 1997.
- [13] P. Misra and P. Enge, *Global Positioning System: Signals, Measurements, and Performance*. Lincoln, MA: Ganga-Jamuna Press, 2001.
- [14] C. Hackman, J. Levine, T. Parker, D. Piester, and J. Becker, "A new technique for estimating frequency from GPS carrier-phase time transfer data," in *Proc. IEEE Int. Ultrason., Ferroelect., Freq. Contr. 50th Anniversary Joint Conf.*, 2004, pp. 341-349.
- [15] D. W. Allan, M. A. Weiss, and J. L. Jespersion, "A frequency-domain view of time-domain characterization of clocks and time and frequency distribution systems," in *Proc. 45th Annu. IEEE Freq. Contr. Symp.*, 1991, pp. 667-678.
- [16] S. Weyers, personal communication, 2004-2005.
- [17] G. Petit, personal communication, 2005.



Christine Hackman was born in Covington, KY. She received bachelor of science degrees in physics and mathematics from Thomas More College, Crestview Hills, KY, and a Ph.D. degree in physics from the University of Colorado, Boulder, CO.

Dr. Hackman is a senior research associate at the University of Colorado, where she performs studies in GPS carrier-phase frequency transfer. Prior to that, as a physicist at the National Institute of Standards and Technology (also in Boulder), she focused on the performance of two-way satellite time and frequency transfer. As a graduate student, she used GPS carrier-phase geodesy and boundary element modeling to study the geodynamics of Iceland.

Her research interests include high-precision time/frequency transfer, geodesy, relativistic effects in orbiting clocks, and applied math.



Judah Levine was born in New York City in 1940. He received a Ph.D. degree in physics from New York University in 1966. He is currently a physicist in the Time and Frequency Division of the National Institute of Standards and Technology (NIST) in Boulder, CO. He is a Fellow of JILA, which is operated jointly by NIST and the University of Colorado at Boulder.

Currently he is studying new methods for distributing time and frequency information using digital networks such as the Internet

and ways of improving satellite-based time and frequency distribution.

Dr. Levine is a Fellow of the American Physical Society and is a member of the American Geophysical Union and the IEEE Computer Society.



Thomas E. Parker (M'79–SM'86–F'94) was born in Natrona Heights, PA, on September 17, 1945. He received his B.S. degree in physics from Allegheny College, Meadville, PA, in 1967. He received his M.S. degree in 1969 and his Ph.D. degree in 1973, both in physics, from Purdue University, West Lafayette, IN.

In August 1973, Dr. Parker joined the professional staff of the Raytheon Research Division, Lexington, MA. Initially, his work was primarily related to the development of improved temperature-stable surface acoustic wave materials. From 1977, Dr. Parker contributed to the development of high-performance surface acoustic wave (SAW) oscillator technology at the Research Division, including the "All Quartz Package" for SAW devices. His primary interest was frequency stability, with an emphasis on $1/f$ noise, vibration sensitivity, and long-term frequency stability. In June 1994 Dr. Parker joined the Time and Frequency Division of the National Institute of Standards and Technology (NIST) in Boulder, CO. He is the leader of the Atomic Frequency Standards Group. His interests include primary frequency standards, time scales, and time-transfer technology. He has been instrumental in incorporating hydrogen masers into the NIST time scale, improving the two-way satellite time and frequency transfer (TWSTFT) system, and in making high accuracy frequency comparisons between primary frequency standards.

Dr. Parker is a Fellow of the IEEE, and a member of Sigma Xi and Sigma Pi Sigma. He has served as an elected member of the Administrative Committee of the IEEE Ultrasonics, Ferroelectrics, and Frequency Control Society (1988–1990 and 2000–2003), and as Chair of the Frequency Control Standing Committee of the UFFC-S (1989–1997). He has served on the Technical Program Committees of both the Ultrasonics and the Frequency Control Symposia. He was the Technical Program Committee Chair for the Frequency Control Symposium in 1990 and 1991 and the General Chair in 1997 and 1998. Dr. Parker also served as the Associate Editor for Frequency Control–Acoustics of the IEEE Ultrasonics, Ferroelectrics, and Frequency Control Society (UFFC-S) Transactions from 1993 to 2003. He received the 1988 Outstanding Transactions Paper Award from the IEEE UFFC-S as a co-author of two papers that appeared in the May 1988 and November 1988 issues of the Transactions. Dr. Parker was the recipient of the Thomas L. Phillips "Excellence in Technology Award" from Raytheon in 1992. In 1994 he received the W. G. Cady Award presented by the IEEE International Frequency Control Symposium. He was the 1996 Distinguished Lecturer for the IEEE

UFFC-S and received the 1999 Achievement Award from the IEEE UFFC-S. In 2003 Dr. Parker received the European Frequency and Time Award from the Societe Chronometrique de France (a sponsor of the European Frequency and Time Forum).



Dirk Piester was born in Salzgitter, Germany, in 1969. He received the Diplom-Physiker and Ph.D. degrees from the Technical University Braunschweig, Braunschweig, Germany, in 1999 and 2002, respectively. His work was focused on the design and characterization of nanostructures in semiconductor devices. Before he began his study of physics, he worked as a technician for power supply electronics at the Siemens AG. Since 2002, he has been with the time dissemination group of the Physikalisch-Technische Bundesanstalt (PTB) where he is in charge of PTB's time dissemination services.

Dr. Piester's main interest is time and frequency transfer via navigation and telecommunication satellites. He presently works on improvements of time transfer technology and calibration techniques. He is member of the German Physical Society.



Jürgen Becker was born in Braunschweig, Germany, in 1968. He received the Diplom-Ingenieur (FH) degree from the Fachhochschule Ostfriesland, Emden, Germany, in 1996. Prior to beginning his study of engineering physics, he performed an apprenticeship as a physics laboratory technician at the Physikalisch-Technische Bundesanstalt (PTB) in Braunschweig.

From 1996 to 1998 he worked in a PTB group that studies flameproof and explosion-proof enclosures. Since 1998 he has worked in the PTB's time dissemination group where he is responsible for the technical aspects of PTB's time dissemination services. Mr. Becker won second place in the 1991 provincewide skills competition conducted by the Industrie- und Handelskammer (IHK) of Lower Saxony.